

Zn Diffusion and α -Fe(Zn) Layer Growth During Annealing of Zn-Coated B Steel

Janik, V, Lan, Y, Beentjes, P, Norman, D, Hensen, G & Sridhar, S

Author post-print (accepted) deposited by Coventry University's Repository

Original citation & hyperlink:

Janik, V, Lan, Y, Beentjes, P, Norman, D, Hensen, G & Sridhar, S 2015, 'Zn Diffusion and α -Fe(Zn) Layer Growth During Annealing of Zn-Coated B Steel' *Metallurgical and Materials Transactions A: Physical Metallurgy and Materials Science*, vol 47, no. 1, pp. 400-411

<https://dx.doi.org/10.1007/s11661-015-3203-y>

DOI 10.1007/s11661-015-3203-y

ISSN 1073-5623

ESSN 1543-1940

Publisher: Springer

The final publication is available at Springer via <http://dx.doi.org/10.1007/s11661-015-3203-y>

Copyright © and Moral Rights are retained by the author(s) and/ or other copyright owners. A copy can be downloaded for personal non-commercial research or study, without prior permission or charge. This item cannot be reproduced or quoted extensively from without first obtaining permission in writing from the copyright holder(s). The content must not be changed in any way or sold commercially in any format or medium without the formal permission of the copyright holders.

This document is the author's post-print version, incorporating any revisions agreed during the peer-review process. Some differences between the published version and this version may remain and you are advised to consult the published version if you wish to cite from it.

Zn diffusion and α -Fe(Zn) layer growth during annealing of Zn coated B Steel

Vit Janik¹, Yongjun Lan², Peter Beentjes³, David Norman⁴, Guido Hensen³, Seetharaman Sridhar¹

¹ WMG, University of Warwick, Coventry CV4 7AL, UK

² Tata Steel, R&D, Swinden Technology Centre, Moorgate Road, Rotherham S60 3AR, UK

³ Tata Steel, R&D, IJmuiden Technology Centre, 1970 CA IJmuiden, the Netherlands

⁴ Tata Steel, R&D, Coventry Technology Centre, Coventry CV4 7AL, UK

Keywords: *Zn coated boron steels, hot press forming, heat treatment, FIB lift-out, Zn concentration, 1D FD model, α -Fe(Zn), γ -Fe(Zn)*

Abstract

Direct hot press forming of Zn coated 22MnB5 steels is impeded by micro-cracks that occur in the substrate during the forming process. Since the availability of Zn is a pertinent factor for these cracks to originate, a study was undertaken to estimate the diffusion of Zn across grains and on grain boundaries in the underlying substrate by extensive characterization of annealed samples combined with the development of a Finite Difference Model (FDM) to describe Zn diffusion and the growth of the α -Fe(Zn) during isothermal annealing of Zn coated 22MnB5. The results suggest that the effective diffusion coefficients of Zn are about $5.00 \times 10^{-13} \text{ m}^2\text{s}^{-1}$ in the α -Fe(Zn) layer and $1.13 \times 10^{-14} \text{ m}^2\text{s}^{-1}$ in the underlying γ -Fe(Zn) substrate at 900 °C. With these coefficients, the maximum diffusion depth of Zn within grains ahead of the bulk of the coating is calculated using the FDM and it is about 3 μm . The diffusion depth of Zn on the grain boundaries is estimated to be 6 μm using the Whipple's solution. This diffusion depth is much shorter than the maximum length (15-50 μm) of the micro-cracks formed in absence of liquid phases and in severely stressed conditions,

indicating that the Zn diffusion during annealing is not the only responsible factor for the formation of micro-cracks.

1. Introduction

The automotive industry is facing increasing demands for improved passenger safety and environmental performance [1]. At the same time, there is a continued focus on cost reduction. In steel intensive automotive bodies, the automotive industry has adopted the use of wide variety of steel types to obtain the best mixture between cost and performance. Among these types, hot pressed Ultra High Strength Steels (UHSS) offer massive improvement of passive safety thanks to their ultra-high strength of 1500-2000 MPa. Manufacturing of complex light-weight components (A, B-pillars, roof rails, crash management structures, etc.) from UHSS using direct hot press forming has become increasingly popular [2]. To meet requirement on corrosion resistance UHSS are usually supplied coated either with an Al-Si coating that offers passive corrosion resistance or with a Zn-based coating [3, 4] that provides active cathodic protection.

The most efficient way of manufacturing parts of Zn coated Boron steels would be through direct Hot Press Forming (HPF). In this process a coated blank is austenitized and subsequently formed and quenched in a single press stroke to achieve the desired strength. However, Zn coated 22MnB5 steels are exposed to temperatures of 880-930 °C during the HPF and are known to suffer from different types of cracking [3, 5]. The mechanism of cracking in Zn coated steel is believed to be a combination of: a) cracks initiated inside the coating as a result of different coefficient of thermal expansion of the coating and the substrate [4]; b) mechanical micro-cracks either newly nucleated on the surface or advancing from already cracked coating layer

under the influence of friction [3]; c) Liquid Metal Embrittlement (LME) due to presence of liquid Zn in the coating, [6, 7] and d) embrittlement induced by enrichment of Zn on grain boundaries during the annealing stage of HPF [9].

It has been observed that no liquid is present both in the coating and in the steel substrate if annealing treatment ranging from 180 to 720 s in duration is applied at the annealing temperature prior to the HPF process [3, 4, 6, 9-11]. In this case, LME is completely avoided. However, the maximum depth of the cracks is still around 15-50 μm for severe forming conditions [12].

It is well understood that the Zn-based coating undergoes a series of phase transformations driven by diffusion of Fe into the coating during heating stage before HPF [10]: initial soft Zn rich η -phase (containing 5-6 wt% Fe) is transformed into hard Γ and Γ_1 phases (17-19.5 and 23.5-28.0 wt% Fe respectively) (for details see [10] and the complex phase diagram obtained from THERMOCALC shown in Fig 1). Additionally, the surface layer of the coating is oxidized at the annealing temperatures with complex and morphologically heterogeneous oxide layer formed [11]. The oxidized products may contain Zn, Mn, Si and Al rich oxides depending on the composition of the substrate and the coating. These phase transformations and reactions on the coating surface are accompanied by turbulences of the coated layer at temperatures between 500 and 800 $^{\circ}\text{C}$ with severe outbursts of Zn occurring on the interface between the coating and the substrate, and by formation of some locations with accumulated Zn and possibly increased Zn content [10]. Finally at temperatures above 850 $^{\circ}\text{C}$ the coating will be largely transformed into a solid solution of Zn in α -Fe(Zn) that will grow in thickness with extended stay at the forming temperature [3, 5, 12]. Optimisation of the treatment as described above has been studied to minimize the depth of the micro-cracks formed in industrial Zn coated 22MnB5 sheet.

However the exact mechanisms behind the reduced cracks penetration into the substrate with extended annealing together with the role of Zn distribution across the coating and in the substrate are not yet fully understood [12].

The objective of this work is to assess whether α -Fe(Zn) and/or Zn diffusion into γ -Fe(Zn) during the annealing process prior to forming could potentially lead to embrittlement of the underlying substrate. This is done by an in-depth study on the evolution of the coating and the Zn distribution during annealing from 240 to 600 s prior to HPF at 900°C in combination with the development of a Finite Difference Model (FDM) to describe Zn diffusion and the growth of the α -Fe(Zn) during isothermal annealing of Zn coated 22MnB5.

2. Materials and Methods

2.1 Experimental material and metallography

The material used in this study was Zn coated 22MnB5 steel with a coating weight of approximately 130gr/m² provided by Tata Steel. The total strip thickness was 1.65 mm. Strips of this material were placed in a roller hearth furnace with air atmosphere heated to 900°C prior to HPF for 240, 300, 480, and 600 s respectively. The experimental stamping process was applied after different isothermal holding times to form U-shaped profiles with drawing depth of 50 mm, draw gap and spacer distance of 0.15 mm, die radius of 2 mm and forming speed of 300 mm/s.

Metallographic samples were obtained from the non-deformed top outer wall of HPF profiles as described in detail in our previous paper - see figure 1 in [12]. Standard metallographic methods for sample preparation were applied; the final etching step depended on the type of analysis performed: (i) non-etched for Scanning Electron Microscope (SEM) Back Scattered Electron imaging (BSEI) and Energy

Dispersive Spectroscopy (EDS) data collection (mapping, line-scans and point analysis); (ii) etched in saturated solution of picric acid in ethanol and wetting agent at 75°C to reveal prior austenite grain boundaries; or (iii) etched in 1% picral followed by 1 % nital for Optical Microscopy (OM) and SEM Secondary Electron imaging (SEI) to analyse the coating/substrate interface, development of the coating thickness and the coating grain size. OM Zeiss Axio Scope A1 and SEM Carl Zeiss Gemini with EDS were used. FIB lift-out method at JEOL 4500 Focused Ion Beam (FIB) SEM was applied on polished cross sections to prepare sections for further TEM analysis. First, locality on the coating/substrate interface containing α -Fe(Zn) grains and prior austenite grain was protected by a C layer to prevent ion milling of the surface, then cross-section lift-out samples and in-plane sections of area about $10 \times 10 \mu\text{m}$ were taken out and attached to a Cu grid, finally FIB ion thinning was applied to prepare 100 nm thin foils for TEM. JEOL 2000FX and JEOL 2100 with EDS operating at 200 kV were used to analyse the FIB cross- and in-plane sections. Additional elemental line scans and mapping were performed by JEOL 2100 operating in STEM mode with spot size of 5.5 nm.

2.2 Diffusion model, assumption and conditions

During heating from the room temperature to the forming temperature 900 °C complex phase transformations involving various Zn-Fe intermetallic phases take place depending on the heating rate [10], making it extremely difficult to experimentally validate numerical models. On the other hand, during the isothermal holding at the forming temperature of 900 °C in duration from 240 to 600 s, a three layer structure is found with the innermost being martensitic substrate (identified here as γ -Fe(Zn), referring to the austenitic state of the substrate at annealing temperature), the middle α -Fe(Zn) coating and the outermost oxide ZnO [12]. Since only three

phases are present during the isothermal annealing the isothermal stage is therefore chosen to be simulated in this work.

The diffusion of Zn within α -Fe(Zn) layer and γ -Fe(Zn) substrate at 900 °C is schematically shown in Fig. 2 with the substrate on the left, the α -Fe(Zn) coating layer in the middle and the Zn oxide on the right side. During annealing Zn diffuses from the interface S_2 into the γ -Fe(Zn) substrate through the α -Fe(Zn) layer. The speed of the interface S_1 is calculated using the Stefan condition [reference to Stefan??] as

$$v|_{x=S_1} = (D_{Zn}^{\gamma} \frac{\partial C_{Zn}^{\gamma}}{\partial x} - D_{Zn}^{\alpha} \frac{\partial C_{Zn}^{\alpha}}{\partial x}) / (C_{Zn}^{\alpha/\gamma} - C_{Zn}^{\gamma/\alpha}) \quad (1)$$

with D_{Zn}^{γ} , D_{Zn}^{α} effective diffusion coefficients in the γ -Fe(Zn) substrate and the α -Fe(Zn) layer, C_{Zn}^{γ} , C_{Zn}^{α} concentrations of Zn in these two phases, $C_{Zn}^{\alpha/\gamma}$, $C_{Zn}^{\gamma/\alpha}$ equilibrium concentrations at both sides of the α - γ interface S_1 . On the right hand side of equation (1), the concentration gradients $\frac{\partial C_{Zn}^{\gamma}}{\partial x}$, $\frac{\partial C_{Zn}^{\alpha}}{\partial x}$ within the γ and α phase

interiors are controlled by the Fick's second law, as shown below

$$\frac{\partial C}{\partial t} = D \frac{\partial^2 C}{\partial x^2} \quad (2)$$

where C , D are Zn concentration and effective diffusion coefficient either in the γ -Fe(Zn) substrate or in the α -Fe(Zn) coating layer, t is time and x is space coordinate.

An one Dimensional (1D) implicit Finite Difference Method (FDM) was developed to solve equation (2) together with the moving boundary condition (equation (1)) for calculating Zn concentration within the α -Fe(Zn) coating layer and the γ -Fe(Zn) substrate during annealing. Fig. 3 shows the starting Zn concentration used in the 1D FDM, which is mapped using the measured data (EDS line scan) for

annealing at 900 °C for 240 s furnace time. The initial average thickness of the α -Fe(Zn) coating layer in the model is 17.8 μm taken from [Table 1](#). The 1D FDM is then used to calculate Zn concentration in the α -Fe(Zn) coating layer and the γ substrate annealed for 300, 480 and 600 s at this temperature. The calculated concentration profiles and α -Fe(Zn) layer thickness are validated by comparing to the corresponding measured values.

In the FDM, the following assumptions are made on the boundary conditions and the diffusion coefficients:

- the interface S_2 is planar and stationary and the Zn diffusion flux across S_2 is equal to zero because the measured weight change shows only thin layer of coating (about 2.0 μm thick) is oxidized during the annealing time from 240 to 600 s and that the oxidation kinetics is approximately linear;
- the interface S_1 is also planar and the boundary conditions are determined using equation (1);
- Zn Diffusion coefficients in the α -Fe(Zn) layer and in the γ -Fe(Zn) substrate are independent on Zn contents in these two phases and are taken thus as constants; and
- on the start of diffusion coefficient calibration the published lattice diffusivity of Zn in the α -Fe(Zn) layer [\[13\]](#) is used, however no data for the diffusivity of Zn in the γ -Fe(Zn) substrate are reported in literature thus the lattice diffusion coefficient of Fe in γ -Fe [\[14\]](#) is used.

Space step size 0.1 μm and time step size 0.001 s are used in all the calculations.

3. Results

3.1 Morphology of the coating

Fig. 4a shows the near surface micro-structure of the top undeformed wall of the U-shaped profile obtained in un-etched condition by BSEI after heating at 900°C for 240 s. This section, unlike the side walls of the final U-shape profile, was not exposed to friction and did not receive any drawing during HPF either. The micrograph demonstrates three different regions present inside the coating: the top Oxide Layer (OL) of 1-3 μm in thickness, $\alpha\text{-Fe(Zn)}$ layer is in the middle and the martensitic substrate (m) at the bottom. It is apparent that the coating is cracked but the cracks do not penetrate into the martensitic substrate. Since top wall was not in contact with the die and not drawn, these cracks might be formed during quenching after forming due to the difference of thermal expansion between the coating and the substrate. **Fig. 4b** illustrates the microstructure after etching in Picral/Nital with visualized grain boundaries of $\alpha\text{-Fe(Zn)}$. Additional elemental maps of Zn by SEM-EDS are shown in **Figs. 4c, 4d**. At short annealing time it is clearly visible that the $\alpha\text{-Fe(Zn)}$ /substrate interface is "wavy" with occurrence of waves corresponding to the grain boundaries separating $\alpha\text{-Fe(Zn)}$ grains. With increasing annealing time the wavy interface becomes less apparent. **Table 1** summarizes measurements of the average thickness of the OL, depth of the $\alpha\text{-Fe(Zn)}$ layer, average size of the columnar $\alpha\text{-Fe(Zn)}$ grains and of the prior austenite grain size. Apart from the growth of the thickness of $\alpha\text{-Fe(Zn)}$ layer all other microstructural parameters are not greatly influenced by increased annealing time – differences are lower than the standard

deviation which is large due to significant heterogeneities of the coating morphology occurring earlier during turbulent events while galvannealing treatment is applied [10].

Further details of the interface morphology at 240 s are provided in Fig. 5a taken by SEI. Faceted interface is apparent coinciding with α -Fe(Zn) grain boundaries. Zn EDS map in Fig. 5b shows possible Zn rich pocket associated with α -Fe(Zn) grain boundary and Fig. 5c shows EDS Zn line scan across the α -Fe(Zn) grain boundary with increased Zn in the vicinity of the grain boundaries. At longer annealing times Zn pockets were not detected by SEM-EDS.

3.2 Zn Distribution in the coating, substrate and at the interface

To be able to measure the Zn concentration both inside the α -Fe(Zn), inside the substrate, and at the α -Fe(Zn)/substrate interface both SEM and high resolution TEM-EDS lines scans were performed. Fig. 6a shows area selected prior to the in-plane FIB lift-out, with grain boundary between the α -Fe(Zn) grains and boundary between the α -Fe(Zn) and the substrate all visible. Corresponding TEM bright field image is shown in Fig 6b and the HR-TEM EDS Zn line scan is in Fig. 6c. HR-TEM EDS Zn profile shows sharp drop in the Zn concentration across the α -Fe(Zn)/substrate boundary which is observed across length of less than 700 nm.

Zn profiles measured by HR-TEM and FEG-SEM EDS for all heating conditions are summarized in Fig. 7a and details of the immediate interface are in Fig. 7b. Measured concentrations C_{Zn}^{α} of Zn in the bulk of α -Fe(Zn) near the top of the coating, C_{Zn}^{γ} of Zn in γ -Fe(Zn) and concentrations $C_{Zn}^{\alpha/\gamma}$, $C_{Zn}^{\gamma/\alpha}$ at both sides of the α - γ interface are presented in Table 2.

3.3 Calculated Zn concentration profiles

Table 3 shows the equilibrium concentrations of Zn at both sides of the α - γ interface S_1 used in the calculations together with the calibrated effective diffusion coefficients in the α -Fe(Zn) coating and the γ -Fe(Zn) substrate.

Fig. 8 shows the calculated Zn concentration profiles across the α -Fe(Zn) and γ -Fe(Zn) phases using the FDM as well as the corresponding measured values using EDS (**obtained from Fig. 7a**). It should be noted that the α - γ interface in **Figs. 8a~8c** is placed to the coordinate origin 0 in order to compare the concentration around this interface. In the FDM this interface S_1 moves into the γ -Fe(Zn) substrate. Results show good agreement between the calculation and the measurement for the Zn concentration (**Figs. 8a~8c**) and reasonable agreement for the α layer thickness (**Fig. 8d**). The α -Fe(Zn) thickness after 480 and 600 s of annealing is about 2.0 μm thicker in the FDM than in the measurement because the oxidation of α -Fe(Zn) coating layer from 240 to 600 s is not considered in the model, as described before.

Results in **Fig. 8** show that Zn concentration in the α -Fe(Zn) layer decrease with annealing time, but both the Zn concentration and the diffusion distance in the γ -Fe(Zn) substrate increase with annealing time. It can also be seen that the thickness of α -Fe(Zn) coating layer increases from 240 to 600 s.

The good agreement between the calculated and the measured Zn concentrations at the distance 20~25 μm to the α - γ interface in **Figs. 8a~8c** implies that the boundary conditions (zero diffusion flux) set at the oxide- α -Fe(Zn) interface S_2 is reasonable. Both calculated and measured Zn concentrations are not lower at the oxide/ α -Fe(Zn) interface S_2 than at other locations within the α -Fe(Zn) coating layer. These results indicate that the depletion of Zn in the α -Fe(Zn) coating layer due to oxidation is little for 240 to 600 s annealing at 900 °C.

It is shown in Figs. 8a~8c that the calculated and the measured Zn concentrations at the distance 10~25 μm to the α - γ interface decrease from about 31wt% for 300 s annealing to about 25wt% for 480 s annealing, but they remain to 25wt% approximately from 480 to 600 s, which means that the equilibrium concentration at the α side of α - γ interface is close to the value (20wt%) used in the calculation. Otherwise Zn concentration in the α -Fe(Zn) coating layer should decrease from 480 to 600 s.

The calculated and the measured Zn concentrations in the γ -Fe(Zn) substrate at the distance -5~0 μm to the α - γ interface) are also in good agreement. This comparison suggests that the equilibrium concentration at the γ side of α - γ interface is about 7.5wt%, as used in the calculation.

The results shown in Figs. 8a~8c indicate that, for the conditions examined, Zn in the α -Fe(Zn) coating layer diffuses, primarily from the oxide- α -Fe(Zn) interface S_2 to the α - γ interface S_1 then further into the γ -Fe(Zn) substrate. Oxidation is slowed down to an extent that Zn is not extracted out of the α -Fe(Zn) for oxidation. This diffusion flux results in a decrease of the Zn concentration in the coating layer until it reaches to the equilibrium concentration. On the other hand, this diffusion flux increases the concentration within the γ -Fe(Zn) substrate. It is found that little Zn (about 1.3 μm) diffuses into the substrate after 300 s annealing. But the diffusion distance in the γ -Fe(Zn) phase increases to about 2.6 and 3.3 μm after 480 and 600 s annealing.

4. Discussion

4.1 Choice of D

In order to calibrate the effective diffusion coefficients of Zn in the α -Fe(Zn) coating layer and in the γ -Fe(Zn) substrate, four 1D FDM simulations are carried out by changing the values for D_{Zn}^{α} and D_{Zn}^{γ} . Fig. 9 shows the sensitivity of Zn concentration profiles and α -Fe(Zn) layer thickness on diffusion coefficients. When the diffusion coefficient D_{Zn}^{α} increases from 1.11×10^{-14} to $5.00 \times 10^{-13} \text{ m}^2\text{s}^{-1}$ with $D_{Zn}^{\gamma} = 1.13 \times 10^{-17} \text{ m}^2\text{s}^{-1}$ fixed, Zn concentration in the α -Fe(Zn) layer becomes lower, but the concentration in the γ -Fe(Zn) phase remains unchanged with an obvious increase observed in the α -Fe(Zn) layer thickness. When the diffusion coefficient D_{Zn}^{γ} increases from 1.13×10^{-17} to 1.13×10^{-13} through $1.13 \times 10^{-14} \text{ m}^2\text{s}^{-1}$ with $D_{Zn}^{\alpha} = 5.00 \times 10^{-13} \text{ m}^2\text{s}^{-1}$ fixed, Zn concentration in the γ -Fe(Zn) substrate increases a lot, but the value in the α -Fe(Zn) layer remains almost unchanged with an apparent decrease seen in the α -Fe(Zn) layer thickness. The calculated Zn concentration profiles both in the α -Fe(Zn) layer and in the γ -Fe(Zn) substrate using $D_{Zn}^{\alpha} = 5.00 \times 10^{-13}$ and $D_{Zn}^{\gamma} = 1.13 \times 10^{-14} \text{ m}^2\text{s}^{-1}$ are in good agreement with the corresponding measured values, as shown in Figs. 8a~8c. The calculated α -Fe(Zn) layer thickness for 480 and 600 s annealing is, however higher than the measured mean values by 2.0 μm , as shown in Fig. 8d. Experimental data show that about 2.0 μm oxide formed during 240 to 600 s annealing, which is not considered in the calculation. Therefore the calculated thickness should be thicker than the measured one by about 2.0 μm .

Table 4 compares the calibrated diffusion coefficients to those reported in Refs [13-15]. The lattice diffusion coefficient of Zn in the γ -Fe(Zn) phase is calculated using $D_{\gamma-Fe}^{Fe} = 5.0 \times 10^{-5} \exp[-284000/(RT)]$ [14], which is the diffusivity of Fe in γ -Fe with R gas constant and T temperature in Kelvin, because no experimental

data for Zn diffusion in the γ -Fe(Zn) are found in literature. The grain boundary diffusion coefficient in the γ -Fe(Zn) substrate is also calculated using the above equation but with the activation energy assumed to be $0.6 \times 284000 = 170400 \text{ Jmol}^{-1}$. It is shown that the calibrated effective Zn diffusion coefficients in the α -Fe(Zn) layer and in the γ -Fe(Zn) substrate are in between the reported data for lattice diffusion and grain boundary diffusion.

The ratio of calibrated effective Zn diffusion coefficients in the α -Fe(Zn) and γ -Fe(Zn) phases is about 44, which is bigger than the reported value (29) for carbon lattice diffusion but smaller than the reported one (165) for iron lattice diffusion, as shown in [Table 5](#). In [Fig. 9d](#) it seems that the calculated α -Fe(Zn) layer thickness using $D_{Zn}^{\gamma} = 1.13 \times 10^{-13} \text{ m}^2\text{s}^{-1}$ is closer to the measured value than the one using $D_{Zn}^{\gamma} = 1.13 \times 10^{-14} \text{ m}^2\text{s}^{-1}$. However, the ratio of $D_{Zn}^{\alpha} / D_{Zn}^{\gamma}$ ($5.00 \times 10^{-13} / 1.13 \times 10^{-13} \approx 4$) becomes even lower than the ratio (29) for carbon lattice diffusion, which is unreasonable. Furthermore, the calculated Zn concentration in the γ -Fe(Zn) substrate is much higher than the corresponding measured values. $D_{Zn}^{\gamma} = 1.13 \times 10^{-14} \text{ m}^2\text{s}^{-1}$ is therefore taken as the calibrated diffusion coefficient in the γ -Fe(Zn) substrate.

4.2 The role of grain boundaries in α -Fe(Zn) and γ -Fe(Zn) on diffusion

The characteristics of the diffusion type of Zn in the α -Fe(Zn) coating layer and in the γ -Fe(Zn) substrate can be determined by comparing the lattice diffusion distance to the mean grain size and grain boundary thickness $\delta \approx 5.0 \times 10^{-10} \text{ m}$ in each of these two phases. When the lattice diffusion distance is significantly smaller than the average grain size, the grain boundary diffusion distance can be estimated using the Whipple's solution [\[16\]](#) as follows

$$\frac{C}{C_0} = \operatorname{erfc}\left(\frac{\eta}{2}\right) + \frac{\eta}{2\sqrt{\pi}} \int_1^{\Delta} \left\{ \sigma^{-3/2} \exp\left(-\frac{\eta^2}{4\sigma}\right) \operatorname{erfc}\left[\frac{1}{2} \sqrt{\frac{\Delta-1}{\Delta-\sigma}} \left(\xi + \frac{\sigma-1}{\beta}\right)\right] \right\} d\sigma$$

$$\Delta = D_{gb} / D_L$$

$$\eta = \frac{y}{\sqrt{D_L t}} \quad (3)$$

$$\xi = \frac{x - \delta/2}{\sqrt{D_L t}}$$

$$\beta = \frac{(\Delta-1)\delta}{2\sqrt{D_L t}}$$

where C/C_0 is normalised concentration, D_{gb} and D_L are grain boundary and lattice diffusivities, δ is grain boundary thickness, t is diffusion time, x and y are space coordinates. **Fig. 10a** shows the geometry used in the Whipple's solution: one grain boundary with two neighboring grains. The normalised concentration profile (C/C_0) along the grain boundary ($x = 0$) is numerically calculated and plotted in the $\eta - \beta$ diagram shown in **Fig. 10b**. The calculated lattice diffusion distance $\sqrt{D_L t}$ and grain boundary diffusion parameter β are shown in **Table 6**.

In the α -Fe(Zn) coating layer, the lattice diffusion distance ($1.6 \mu\text{m} < \sqrt{D_L t} < 2.6 \mu\text{m}$) is slightly smaller than the measured mean grain size (about $10 \mu\text{m}$ – see **Table 1**), but they are in the same magnitude order. The grain boundary diffusion parameter ($1.8 < \beta < 2.9$) is also relatively small. Above results indicate that in the coating layer Zn diffusion after 240 to 600 s annealing is Type AB and very close to Type A (bulk diffusion). Grain boundaries therefore play a certain role for diffusion, but the role is not substantial. The Whipple's solution is therefore not suitable for calculating the diffusion distance in this phase.

In the γ -Fe(Zn) substrate, the lattice diffusion distance ($0.05 \mu\text{m} < \sqrt{D_L t} < 0.09 \mu\text{m}$) is much smaller than the measured mean grain size (about $9 \mu\text{m}$), but apparently

bigger than the typical grain boundary thickness $\delta \approx 5.0 \times 10^{-10} m$. The grain boundary diffusion parameter ($340 < \beta < 550$) is relatively big. These results indicate that in this phase Zn diffusion after 240 to 600 s annealing is Type B, which is in between a bulk diffusion and a grain boundary diffusion. The Whipple's solution can be used to estimate the diffusion distance of Zn along γ -Fe(Zn) grain boundaries. Let's take the annealing at 900°C for 600 s as an example. Estimated grain boundary diffusion parameter

$$\beta = (\Delta - 1)\delta / (2\sqrt{D_L t}) = (1.29 \times 10^{-12} / 1.13 \times 10^{-17} - 1) \times 5.0 \times 10^{-10} / (2 \times \sqrt{1.13 \times 10^{-17} \times 600}) \approx 347 .$$

From Fig. 10b, we can find the corresponding value $\eta \approx 70$. Estimated grain boundary diffusion distance across which the Zn concentration decreases from the equilibrium concentration 7.5wt% down to 0.075wt% is

$$y = \eta \sqrt{D_L t} \approx 70 \times \sqrt{1.13 \times 10^{-17} \times 600} \approx 5.76 \times 10^{-6} m .$$

It should be noted that the Whipple's solution does not consider the moving α - γ phase interface and thus in the above calculated grain boundary diffusion distance (6 μ m) for 600 s annealing is over-estimated.

4.3 Zn diffusion into the γ -Fe(Zn) substrate

The effect of D_{Zn}^γ on the calculated Zn content profiles in the γ -Fe(Zn) substrate, as shown in Figs. 9a~9c, indicates that Zn concentration increases with D_{Zn}^γ with good agreement between calculations and measurements observed when $D_{Zn}^\gamma = 1.13 \times 10^{-14} m^2 s^{-1}$ (see Figs. 8a~8c). Comparing to the measured Zn contents, it is found that $D_{Zn}^\gamma = 1.13 \times 10^{-17} m^2 s^{-1}$ is too small and $D_{Zn}^\gamma = 1.13 \times 10^{-13} m^2 s^{-1}$ is too large. The agreement in the calculated and measured Zn concentrations in the γ -Fe(Zn) substrate (Fig. 8) suggests that the 1D FDM can be used to estimate the leaking of Zn into the bulk substrate: 1.3 μ m for 300 s annealing, 2.6 μ m for 480 s

and 3.3 μm for 600 s in terms of diffusion distance. The diffusion in this phase is Type B, as discussed previously. The grain boundary diffusion distance is longer, i.e. about 6 μm estimated using the Whipple's solution.

4.4 Zn diffusion and the mechanism of micro-cracking

With extended duration of annealing the Zn and Fe inter-diffusion between the coating and the substrate will lead to a flattening out of the Zn drop in the concentration profile and to the reduction of Zn accumulations inside the $\alpha\text{-Fe(Zn)}$ layer (especially at the $\alpha\text{-Fe(Zn)}$ grain boundaries and at $\alpha\text{-Fe(Zn)}$ /substrate triple junctions where Zn waves or pockets of Zn can be observed at lower annealing temperatures and short annealing times (Fig. 6 in [12]). This will reduce the depth of the micro-crack penetration into the substrate. The modelling of Zn distribution with increasing annealing time and calculation of the coating growth is provided to give a predictive tool to enable to access the Zn distribution in the coating at various annealing conditions. This approach if in future incorporated into a mechanistic crack propagation model may lead to a complex design tool which will allow elimination of the problem of cracking in direct HPF of Zn coated steels.

5. Conclusions

- Zn concentration is about 25wt% in the bulk of the $\alpha\text{-Fe(Zn)}$ coating layer after 480 to 600 s annealing at 900 °C and it is about 5wt % at the $\gamma\text{-Fe(Zn)}$ side of the $\alpha\text{-}\gamma$ interface.
- At 900 °C, Equilibrium concentration of Zn is about 20wt% at the α side of $\alpha\text{-}\gamma$ interface and it is between 5~12wt% (about 7.5wt%) at the γ side of $\alpha\text{-}\gamma$ interface.

- At 900°C, effective diffusion coefficient of Zn is about $5.00 \times 10^{-13} \text{ m}^2\text{s}^{-1}$ in the α -Fe(Zn) layer. It is about $1.13 \times 10^{-14} \text{ m}^2\text{s}^{-1}$ in the γ -Fe(Zn) substrate.
- Lattice diffusion distance in the γ -Fe(Zn) substrate increases with annealing time. It increases from about 1.3 μm for 240 s annealing to 3.3 μm for 600 s annealing.
- The thickness of α -Fe(Zn) coating layer is about 18~22 μm after 300~600 s annealing at 900 °C.
- Zn concentration decreases with annealing time in the α -Fe(Zn) coating, whilst it increases with annealing time in the γ -Fe(Zn) phase. The thickness of α -Fe(Zn) coating increases with annealing time between 240 and 600 s.
- Zn concentration in the α -Fe(Zn) coating is predominantly determined by diffusion coefficient D_{Zn}^{α} . The diffusion coefficient D_{Zn}^{γ} in the γ -Fe(Zn) substrate has little effect. Similarly, Zn concentration in the γ -Fe(Zn) substrate is dependent on D_{Zn}^{γ} only. Zn concentration decreases with D_{Zn}^{α} in the α -Fe (Zn) phase, but it increases with D_{Zn}^{γ} in the γ -Fe(Zn) phase.
- The thickness of α -Fe(Zn) coating layer is controlled by the Zn diffusion coefficients both in the α -Fe(Zn) phase and in the γ -Fe(Zn) phase. It increases with the diffusion D_{Zn}^{α} in the α -Fe(Zn) layer but decreases with the diffusion D_{Zn}^{γ} in the γ -Fe(Zn) substrate.
- Zn diffusion in the α -Fe(Zn) coating layer after 300 to 600 s annealing at 900 °C is Type AB and very close to Type A (bulk diffusion), but the diffusion in the γ -Fe(Zn) substrate belongs to Type B, which is in between bulk diffusion and grain boundary diffusion. Zn grain boundary diffusion distance in the γ -

Fe(Zn) substrate after 600 s annealing at 900 °C was estimated to be about 6 μm using the Whipple's solution.

- Both the Zn bulk diffusion distance 3 μm calculated using the FDM and the Zn grain boundary diffusion distance 6 μm estimated using the Whipple's solution indicate that the Zn diffusion during annealing is not the only responsible factor for the formation of micro-cracks that have a maximum depth of 15-50 μm in absence of liquid phases and in severely stressed conditions.
- Reduced amount of Zn-rich pockets at α -Fe(Zn) grain boundaries, flattened out at coating/substrate interface, and reduced zinc concentration in α -Fe(Zn) with increasing annealing time may contribute to the reduced susceptibility to deep micro-cracks formed during the mechanical loading in the samples annealed for longer time, e.g., 480 s and 600 s. However, the increase of Zn concentration and Zn diffusion depth in the γ -Fe(Zn) substrate can not explain the fact: the length of micro-cracks decreases slightly as annealing time increases.

Acknowledgement

Financial assistance from the WMG Centre High Value Manufacturing Catapult with focus on low C mobility and Tata Steel is gratefully acknowledged. The authors are thankful for the assistance from Dr Richard Beanland and Steven Hindmarsh at MAS, University of Warwick with the TEM analysis with FIB lift-out. The authors also wish to thank Dr Didier Farrugia for discussing aspects of the diffusion modelling.

References

- [1] European Automotive Research Partners Association R&D technology Roadmap; http://www.earpa.eu/docs/2005/furore_road_map_final.pdf
- [2] Altan, T, Update: Hot-stamping boron-alloyed steels for automotive parts, Stamping Journal (2011)
- [3] Kim, S., Son, I., Kim, D., Kim, S., Cracking issues of Zn coated Press Hardening Steel in Direct Hot Press Forming, (2013), *4th Int. Conf. on Hot Sheet Met. Forming of UHSS*, Lulea, Sweden.
- [4] Drillet, P., Grigorieva R., Leuillier G., Vietoris T., Study of cracks propagation inside the steel on press hardened steel zinc based coatings, (2011) Galvatech, Genova, Italy
- [5] van Genderen M.J., Verloop, W., Loiseaux, J., Hensen, G.C., Zn-coated Boron steel, Direct hot forming for automotive applications (2011), *3rd Int. Conf. on Hot Sheet Met. Forming of UHSS*, Kassel Germany
- [6] Lee, C.W., Fan, D.W., Sohn, I.R., Lee, S.-J., De Cooman, B.C., Liquid-metal-induced embrittlement of Zn-coated hot stamping steel (2012) *Metal. Mater. Trans. A*
- [7] Lawrence Cho, Heeseung Kang, Changwook Lee, Bruno C. De Cooman, Microstructure of liquid metal embrittlement cracks on Zn-coated 22MnB5 press-hardened steel, *Scripta Materialia*, Available online 24 July 2014, ISSN 1359-6462, <http://dx.doi.org/10.1016/j.scriptamat.2014.07.008>.
- [9] Hensen, G., Melfo, W., Chen, S., Developing Zn coated B steels: balancing microcrack performance and corrosion protection (2013), *4th Int. Conf. on Hot Sheet Met. Forming of UHSS*, Lulea, Sweden.
- [10] Mader, A.R. The metallurgy of zinc-coated steel, *Progress in Materials Science* 45 (2000) 199-271.

[11] Robert Autengruber, Gerald Luckeneder, Siegfried Kolnberger, Josef Faderl, Achim Walter Hassel, Surface and Coating Analysis of Press-Hardened Hot-Dip Galvanized Steel Sheet, steel research international, Volume 83, Issue 11, pages 1005–1011, November 2012

[12] Vit Janik, Peter Beentjes, David Norman, Guido Hensen, Sridhar Seetharaman, Role of Heating Conditions on Micro-crack Formation in Zn-Coated 22MnB5, Proceedings of MST2014 conference, Pittsburgh, USA, 2014

[13] I Richter, M Feller-Kniepmeier, Phys. Status Solidi (A) 68 (1981) 289–300.

[14] Smithells Metals Reference Book, EA Brandes, GB Brook ed, 7th edition, Butterworth & Heinemann, 1992.

[15] JS Dohie, JR Cahoon, WF Caley, JPEDAV 28 (2007) 322-327.

[16] RTP Whipple, Philos Mag 45 (1954) 1225.

Figure captions:

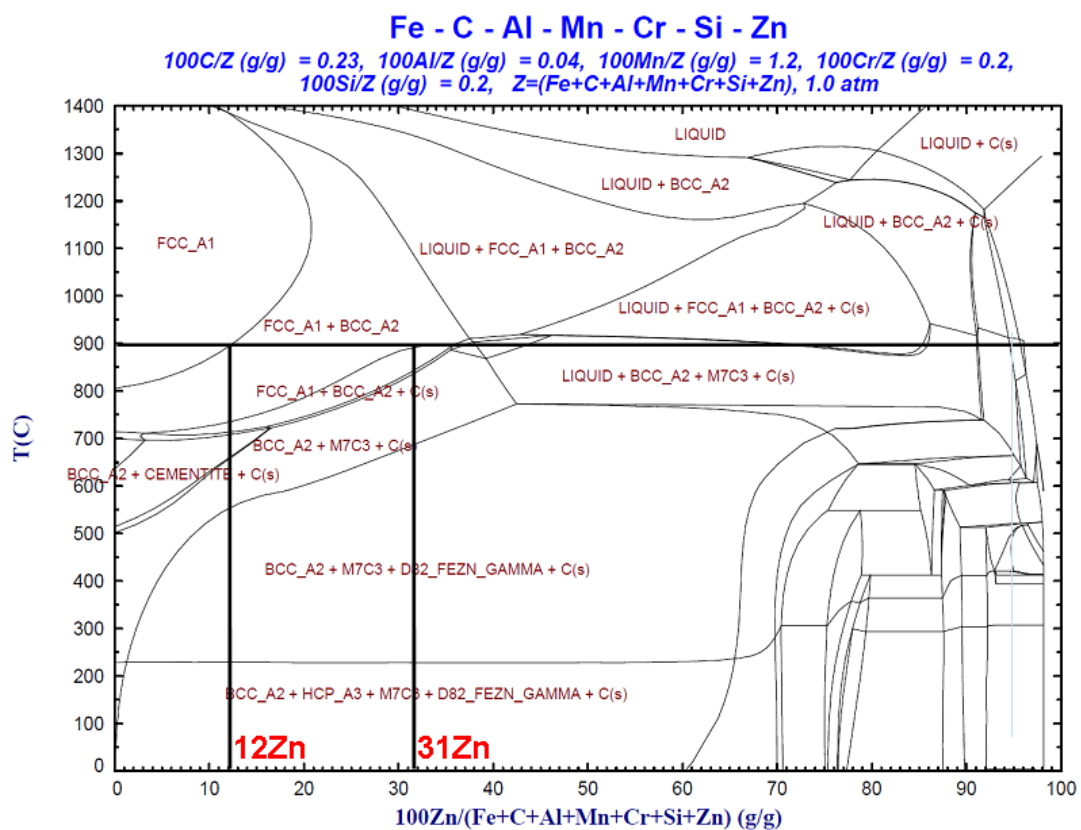


Figure 1: Phase diagram of Fe-C-Al-Mn-Cr-Si-Zn system calculated by THERMOCALC showing phase composition and Zn content in $\alpha(\text{Fe,Zn})$ at 900°C. – DO WE NEED TO CHANGE DESIGNATION TO APPROPRIATE GREEK LETTERS for the paper – *I will ask Sam to run thermocalc and will process the diagram to have a complex one and not just a binary one.*

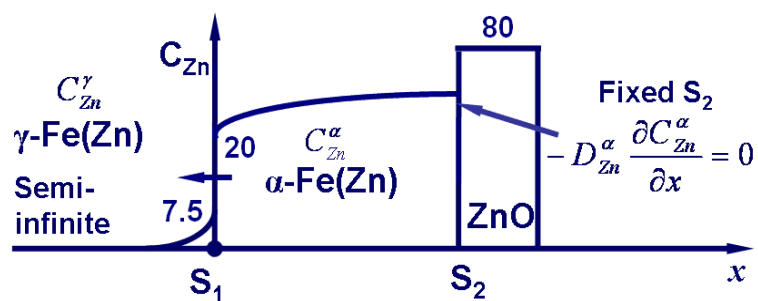


Figure 2 1D model of Zn diffusion at 900°C with S_2 fixed and no Zn flux across S_2 . The equilibrium Zn concentrations (20wt% and 7.5wt%) at both sides of S_1 are also given.

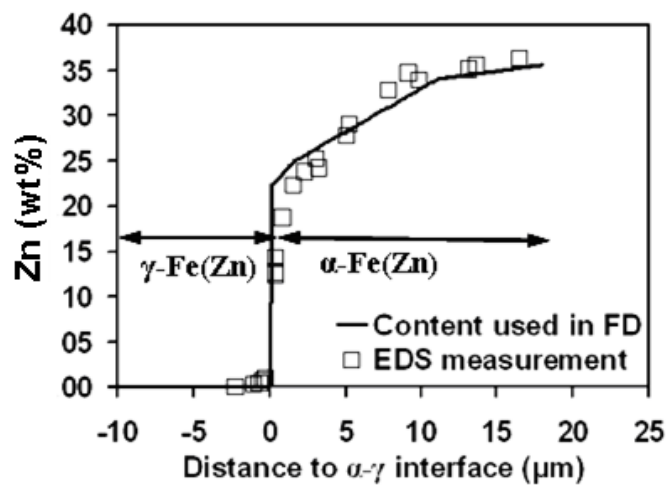


Figure 3 Zn concentration profile used in the 1D FDM (solid line) as start condition of simulation. These model data are mapped using the values of EDS line scan (squares) for the annealing at 900°C for 240 s. The thickness (17.8 μm) of α -Fe(Zn) layer in the model is determined using the average value of measured thickness.

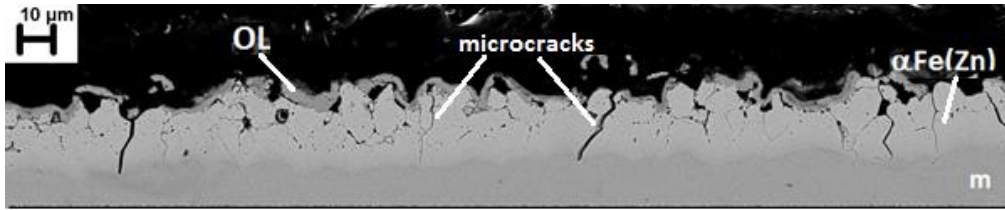
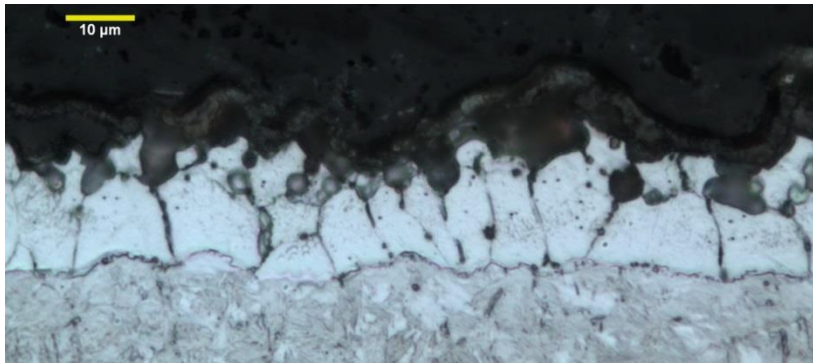
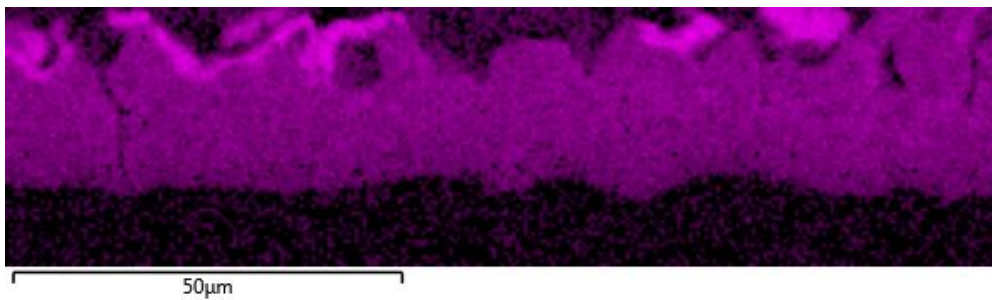


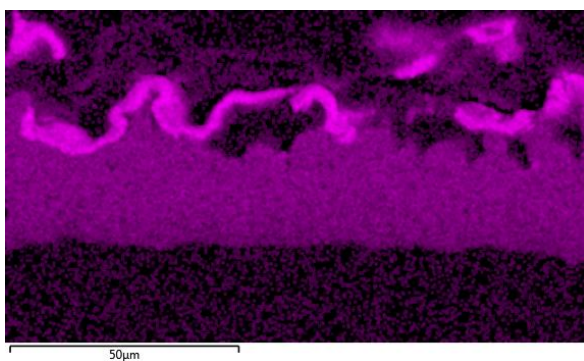
Fig 4a Unetched coating micrograph showing OL, α -Fe(Zn) and substrate by BSEI SEM. Holding time 240 s at temperature 900 °C.



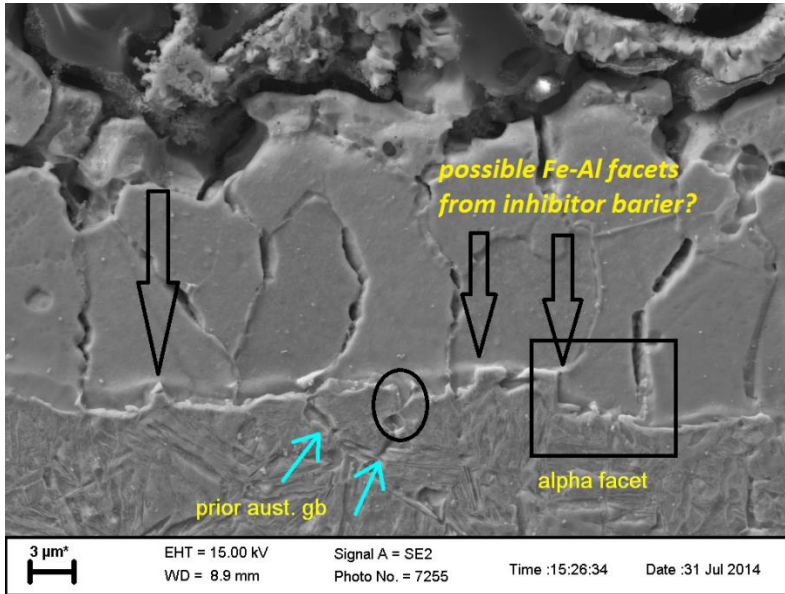
4b OM micrograph of etched coating showing wavy interface between the α -Fe(Zn) layer and the substrate, waves matching the α -Fe(Zn) GBs. Holding time 240 s at temperature 900 °C.



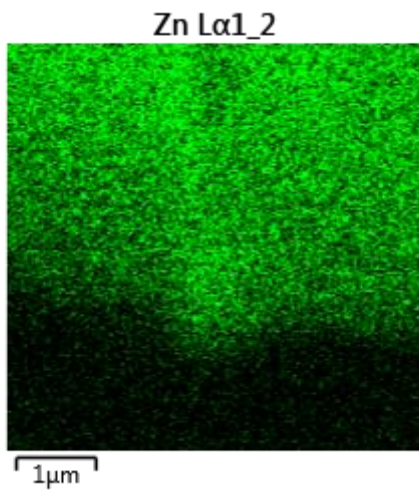
4c – EDS Zn distribution map corresponding to Fig, 4b obtained at holding time 240 s at temperature 900 °C.



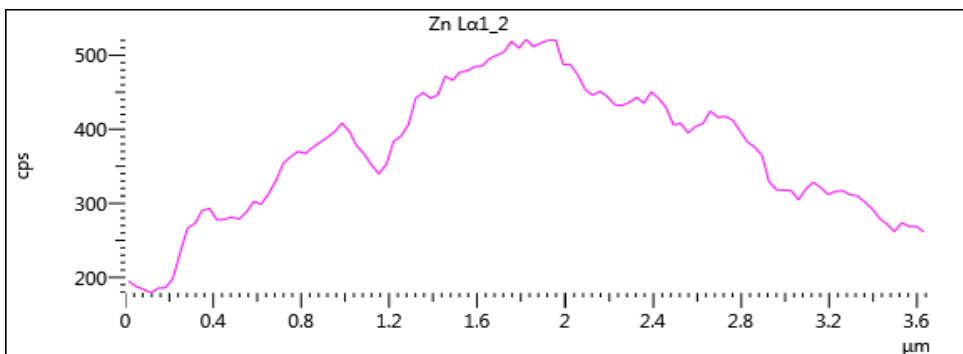
4d EDS Zn distribution map obtained at holding time 600 s at temperature 900 °C showing less wavy interface between the α -Fe(Zn) layer and the substrate. (NB – I will process the pictures to have the same size and appearance later)



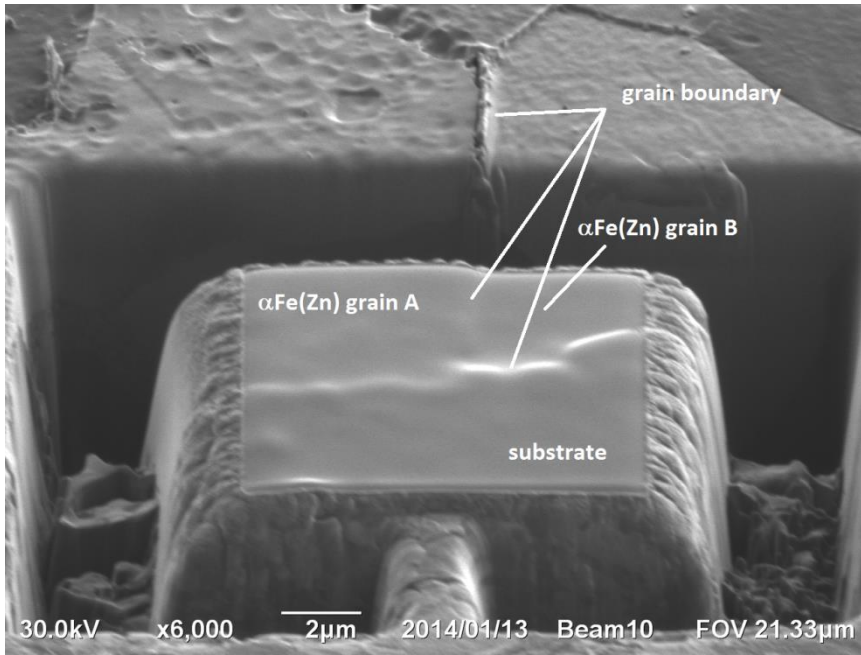
5a) etched coating by SEM with arrows indicating facets and location of Zn pockets 240/900



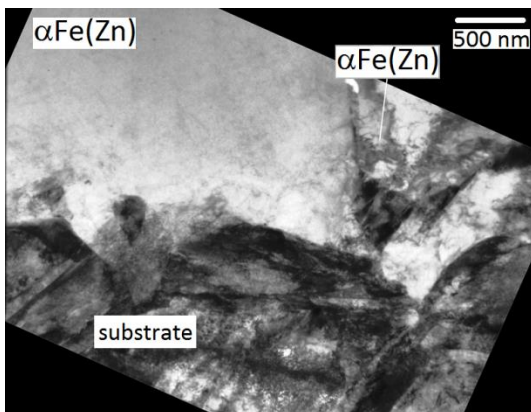
5b) Detailed example of possible Zn pocket an Zn wave at Gb with prior austenite



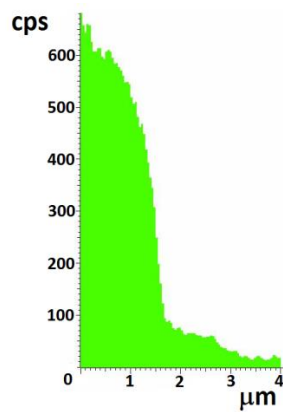
5c) Zn linescan across the pocket



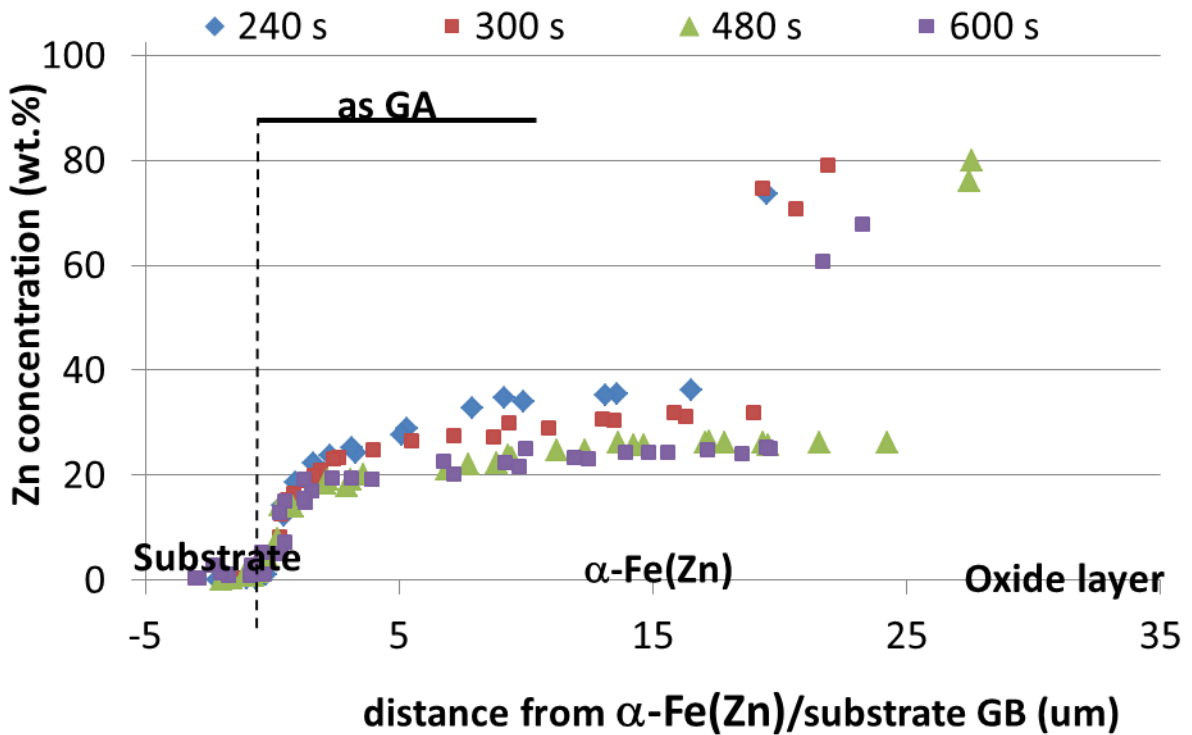
6a) FIB SEM dual beam image showing location of the in-plane lift out sample for TEM separated from the rest of the sample by milled trenches; in-plane lift-out locality is with a C layer applied onto it to protect the surface slightly obstructing the etched microstructural features.



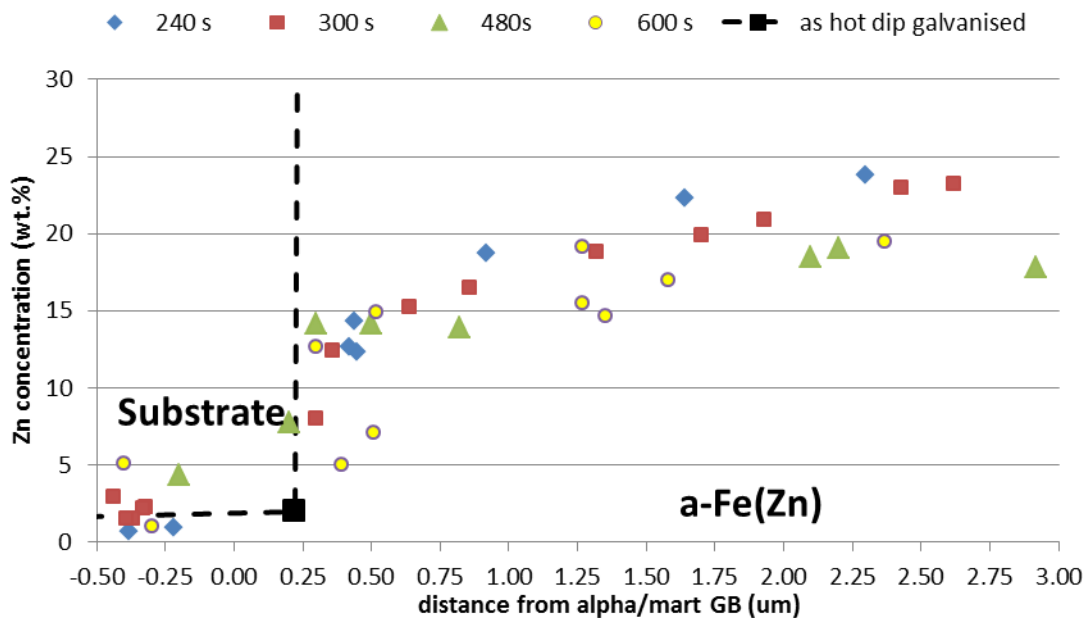
6b) TEM bright field image of a) showing GBs; EDS was collected from this area.



6c) Scanning TEM Zn profile taken from the interface.



7a) Zn distribution profiles acquired by SEM and TEM EDS for all annealing conditions; dashed line showing as hot dip galvanized Zn profile.



7b) detail of the immediate interface – I will process the pics later – don't have them here.

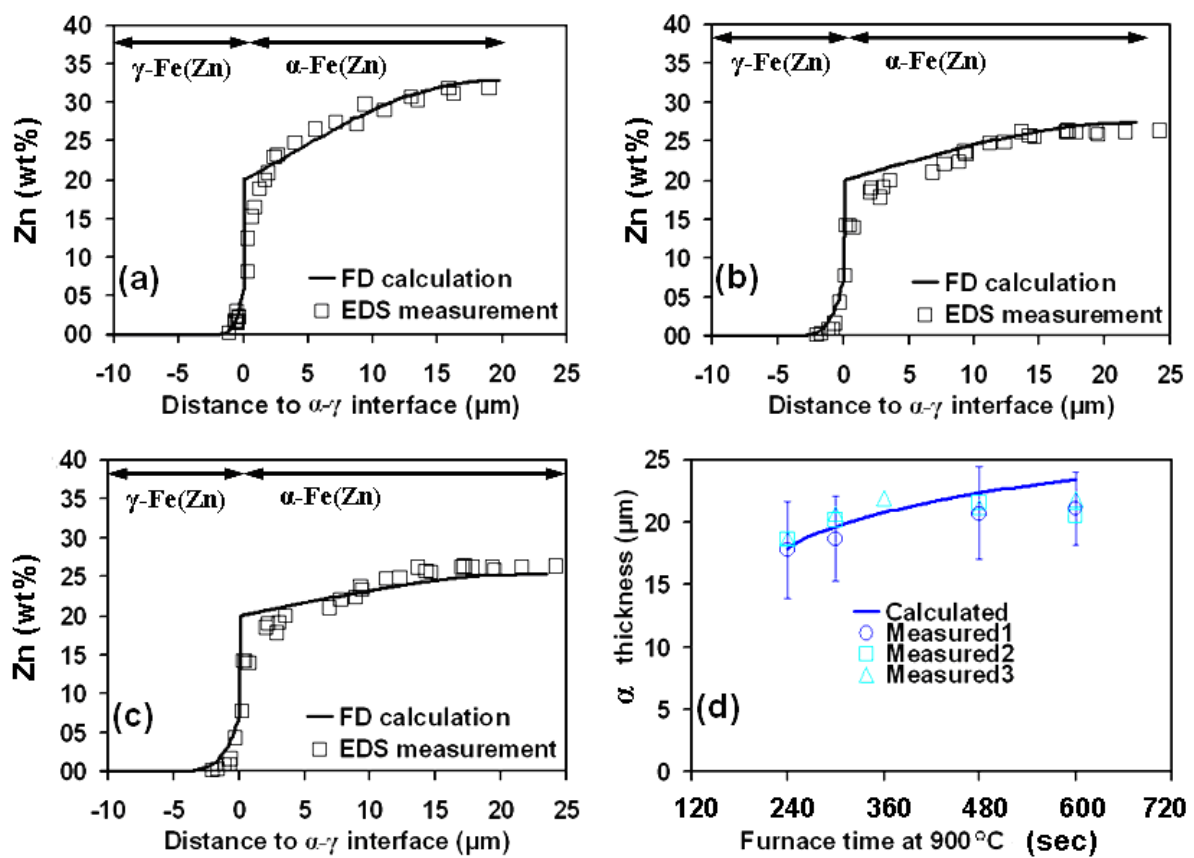


Figure 8 Calculated Zn concentration profiles for different annealing times: (a) 300 s, (b) 480 s and (c) 600 s and calculated α -Fe(Zn) layer thickness (d). Measured Zn concentration using EDS and measured α -Fe(Zn) layer thickness are also given for comparison.

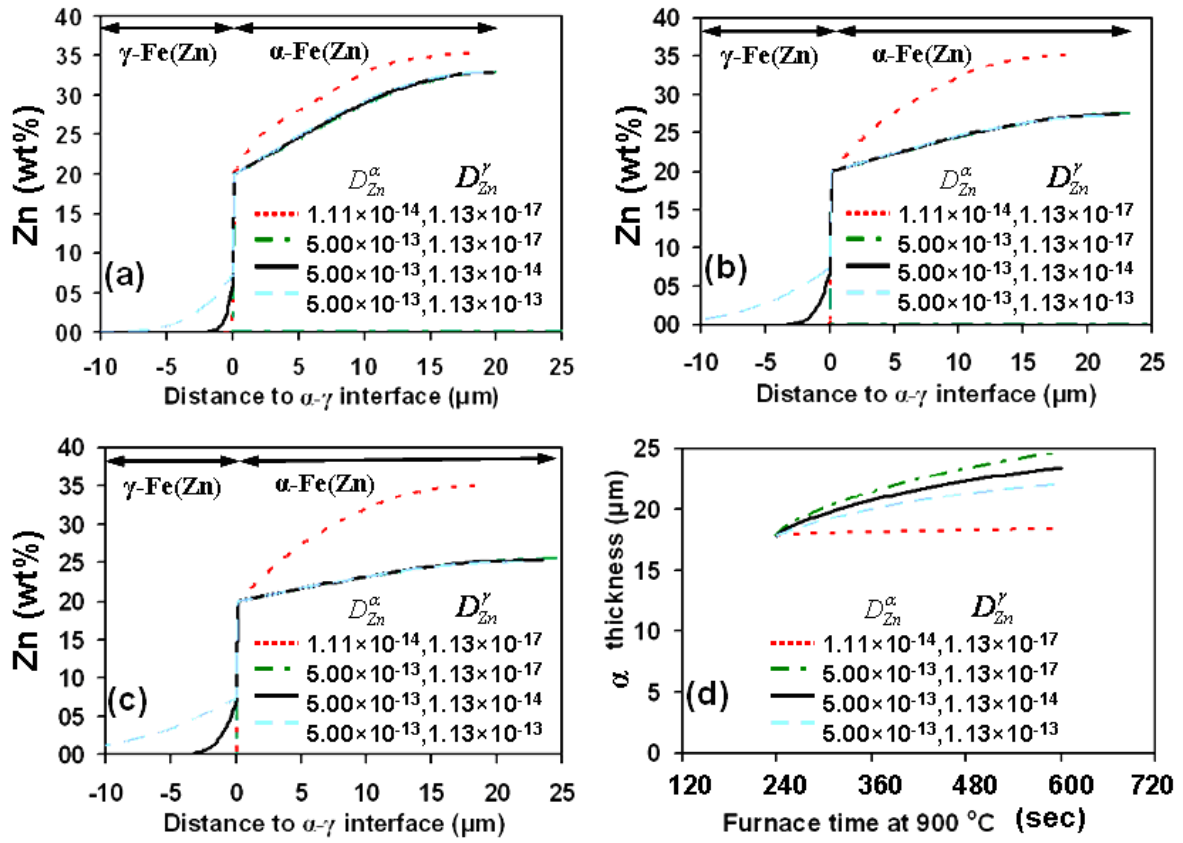


Figure 9 Effect of D_{Zn}^{α} , D_{Zn}^{γ} on calculated Zn concentration profiles: (a) 300 s, (b) 480 s and (c) 600 s and on calculated α -Fe(Zn) layer thickness (d).

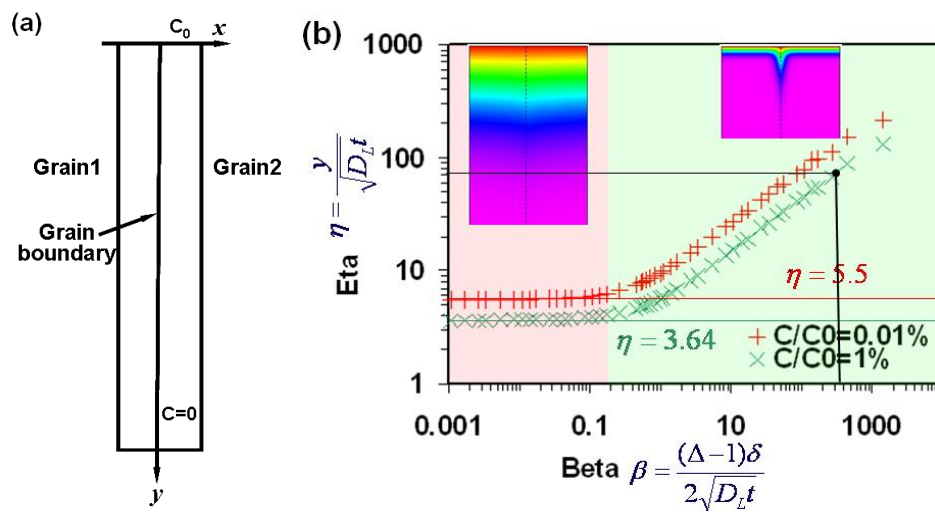


Figure 10(a) Grain boundary geometry used in the Whipple's solution and (b) Whipple's solution plotted using parameters Beta and Eta with $\beta = (\Delta - 1)\delta / (2\sqrt{D_L t})$ and $\eta = y / \sqrt{D_L t}$. Here $\Delta = D_{gb} / D_L$, $\delta \approx 5.0 \times 10^{-10} m$ and y is coordinate along grain boundary. Inserted concentration maps indicate the effect of grain boundaries on diffusion.

Table 1 Average depth of OL and of α Fe(Zn) layer for all heating conditions at T 900C.

time (s)	avg. thickness of OL (μm)	avg. depth α Fe(Zn) (μm)	avg. size of columnar α Fe(Zn) grains (μm)		Avg. size of prior austenite grain (μm)
			avg. length	avg. diameter	
			(μm)	(μm)	
240	2.1 ± 0.9	17.8 ± 3.9	10.9 ± 4.8	7.4 ± 4.5	9.7 ± 1.7
300	2.2 ± 1.0	18.7 ± 3.4	10.7 ± 4.8	7.0 ± 2.8	9.6 ± 2.8
480	2.2 ± 1.2	20.7 ± 3.7	11.9 ± 3.5	7.4 ± 4.7	8.1 ± 3.1
600	2.8 ± 1.6	21.1 ± 2.9	10.6 ± 4.8	6.1 ± 4.8	8.6 ± 3.2

Table 2 – Experimentally observed Zn concentrations

Holding time (s)	Measured Zn concentration in γ -Fe(Zn) wt%		Measured Zn concentration in α -Fe(Zn) wt%	
	C_{Zn}^{γ}	$C_{Zn}^{\gamma/\alpha}$	C_{Zn}^{α}	$C_{Zn}^{\alpha/\gamma}$
	240	0.1<	~1.5	35
300	0.1<	~1.5	30	15<
480	0.1<	~1.5	25	15<
600	0.1<	~1.5	22	15<

Table 3 Model parameters used in equation (1)

900°C	Effective Zn diffusion coefficient (m ² s ⁻¹)	Equilibrium Zn concentration (wt%)
α-Fe(Zn)	5.00×10 ⁻¹³	20
γ-Fe(Zn)	1.13×10 ⁻¹⁴	7.5

Table 4 Comparison of calibrated and reported diffusion coefficients (m^2s^{-1})

900°C	α -Fe(Zn)	γ -Fe(Zn)
D_{Eff} (calibrated)	5.00×10^{-13}	1.13×10^{-14}
D_L	1.11×10^{-14} [13]	1.13×10^{-17} [14] (Fe in γ -Fe)
D_{gb}	2.08×10^{-10} [15]	1.29×10^{-12} [14] (Fe in γ -Fe)

Table 5 Ratios of diffusion coefficients (m^2s^{-1}) between α and γ phases

900°C	D^α/D^γ
Zn (calibrated)	$5.00 \times 10^{-13} / 1.13 \times 10^{-14} \approx 44$
C [14]	$1.70 \times 10^{-10} / 5.90 \times 10^{-12} \approx 29$
Fe [14]	$1.86 \times 10^{-15} / 1.13 \times 10^{-17} \approx 165$

Table 6 Lattice diffusion distance $\sqrt{D_L t}$ and grain boundary diffusion parameter $\beta = (\Delta - 1)\delta / (2\sqrt{D_L t})$ in the α -Fe(Zn) coating layer and the γ -Fe(Zn) substrate with D_L and D_{gb} taken from Table 4

900°C		240 s	300 s	480 s	600 s
α -Fe(Zn)	$\sqrt{D_L t}$ (μm)	1.63	1.82	2.31	2.58
	β	2.87	2.57	2.03	1.82
γ -Fe(Zn)	$\sqrt{D_L t}$ (μm)	0.052	0.058	0.074	0.082
	β	548	490	388	347